JOURNAL OF SPACECRAFT AND ROCKETS
Vol. 32, No. 4, July–August 1995

Pitch Analysis of a Space Module After Water Landing

D. E. Van Sickle* and L. A. Anderson†
University of Central Florida, Orlando, Florida 32816

Dynamic pitch response of a water landing space module (WLSM) during a postsplashdown situation was investigated. Analysis of test results using a one-fifth scale model are reported. Tests were performed for various center of gravity (c.g.) locations with and without use of flotation/stabilization aids. These aids were in the form of attitude spheres attached to the model just below the water line. Data and information obtained from testing established trends for different model configurations. Pitch oscillation increases resulted as the c.g. was offset horizontally. Less significant pitch oscillation increases were observed with an increasing vertical c.g. offset. The application of attitude spheres reduced the pitch oscillations for all c.g. configurations investigated. Measuring the pitch motion of the WLSM in different configurations identifies design parameters useful in smoothing the ride for the sick or injured crewmember in the postsplashdown environment. The results obtained are suggested design considerations for a full-scale WLSM.

Nomenclature

A = constant for general solution of second-order differential equation, rad
a = distance from pivot point to c.g., in.
B = constant for general solution of second-order differential equation, rad
b = linear damping coefficient proportional to velocity, lb/in.^{2}/s
c = restoring coefficient associated with restoring moment, lb/in.^{2}
g = acceleration due to gravity, in./s^2
gm = metacentric height, in.
h = wave height, in.
I = inertia of model (shell and plates together), lb/in.^{2}/s^2
I' = added inertia (effect of water entrained by the model), lb/in.^{2}/s^2
I_G = mass moment of inertia about c.g. of model shell, lb/in.^{2}/s^2
I_w = $I + I'$ = total inertia of model, lb/in.^{2}/s^2
L = wavelength, in.
M = mass of the system, slugs
M_1 = inertial moment, lb/in.^{2}/rad
M_2 = damping moment, lb/in.^{2}/rad
M_3 = restoring moment, lb/in.^{2}/rad
m = mass of model, slugs
m_i = mass of n individual components, slugs
T_d = damped natural period, s
t = time, s
W = weight, lbf
x, y, z = mass center of system (c.g.), in.
x_i, y_i, z_i = mass center of n components, in.
α = phase shift for general solution of second-order differential equation, rad
α_m = maximum waveslope, rad
δ = logarithmic decrement, dimensionless
ε = phase shift in steady-state solution, rad
Θ = angular displacement, rad
$\theta, \theta', \theta''$ = model pitch, rotational velocity, and acceleration, rad, rad/s, and rad/s^2
θ_a, θ_h = steady-state amplitude and homogeneous solution, respectively, rad
τ = period of oscillation, s
ϕ = water line in pitch direction (waveslope), rad
ω = wave frequency, rad/s
ω_n = natural frequency of model, rad/s
ζ = damping coefficient, lb/in.^{2}/rad

Received June 17, 1993; revision received Nov. 9, 1993; accepted for publication Nov. 12, 1993.

*Research Engineer; Rockwell International Research Fellow. Member AIAA.

†Associate Professor, Mechanical and Aerospace Engineering. Associate Fellow AIAA.

Introduction

A WATER landing space module (WLSM) permanently attached to the Space Station is capable of returning the crew members of Earth at any time. The WLSM is envisioned for use in the event of a medical emergency, a Space Station catastrophe, or if the Space Transportation System supplying the space station is interrupted and the crew requires an alternative method of returning to Earth. In the postsplashdown of a water landing, a WLSM demonstrates dynamic characteristics dependent on the sea state and the moment of inertia, and the center of gravity (c.g.) of the WLSM. The purpose of this paper is to examine the pitch stability of a WLSM. Static pool testing and analytical approximations were used to determine the pitch response characteristics of the WLSM. The research also examined the effect of flotation/stabilization aids in the form of inflatable spheres attached just below the waterline.

Postsplashdown studies[1–3] of the manned Apollo missions identified sea and weather conditions that caused severe discomfort to the crew. The Apollo command module (ACM) was a planned return to Earth, and was not intended to spend a long time in the water.[2] The unplanned and unexpected returns of a WLSM result in potentially longer time periods on the water. Longer time periods increase crew discomfort and the probability of incurring motion sickness.

The Apollo studies showed the command module had two stable positions: an upright, stable I, position and an upside down, stable II, position.[2] An uprighting system[3] was developed that eliminated the stable II position. The WLSM is an ACM derivative and has two similar stable positions. The WLSM research assumed a steady-state time frame after impact with the stable I position as the initial condition.

Mass properties of the WLSM model were determined experimentally. A system of steel plates installed in the model allowed a range of c.g. locations. Knowing the model's properties and the position of the plates, various c.g. locations and corresponding mass moments of inertia were obtained analytically.

The WLSM is a symmetrical, free-floating body and was analyzed in the same manner as a buoy. The model was modified by adding flotation attitude spheres along the perimeter, just below the water line. Static pool tests were repeated for a range of c.g. locations with the spheres attached in symmetrical and unsymmetrical arrangements.

The results of the static pool tests were applied to the model's pitch equation of motion, and the pitch response was generated

from the equation of motion using the coefficients obtained in the static testing. The results of the static testing and the corresponding analytical results were generated graphically and compared. Trends revealed during static testing and analytical approximations form the basis for the observations and recommendations.

WLSM Scale Model

The one-fifth scale working model simulates the dynamic behavior of an ACM-based WLSM. Three primary considerations were geometric and dynamic similitude, method for modeling the c.g. and mass moment of inertia, and the mass properties.

Geometric and Dynamic Similitude

The model was scaled down using the Buckingham Pi Theorem for rigid body motion.[4] The model size was chosen to be one-fifth the size of the prototype. The scaling factors are listed in Table 1.

The WLSM model dimensions, which were derived from an ACM derivative, are shown in Fig. 1. The dimensions for the model depict the wet dimensions, the dimensions of an ACM derivative during postsplashdown. The model dimensions represent a possible WLSM design.

Center of Gravity and Mass Moment

To simulate a variety of WLSM designs, it was necessary to construct a subsystem capable of easily varying the position of the c.g. and the magnitude of the mass moment of inertia. Methods of accomplishing this variability were compared and contrasted with respect to their effectiveness and ease of variability.

A system of three flat circular plates was chosen for modeling both the c.g. and mass moment of inertia of the WLSM. This system consists of a fixed flat plate mounted inside the base of the spherical segment shell, a second fixed plate at the top of the apex shell, and a movable center plate system attached to the floor of the model. The system of three flat circular plates can be treated as a concentrated mass with local c.g. at the centroid of the plates. By varying the position of the center plate, the c.g. of the model can be altered for testing. The three-plate system has the final configuration as listed in Table 2.

The middle plate is bolted to the floor of the WLSM model using a system of four studs, spacers, and washers. The plate has a horizontal range from 0 to 3.0 in. away from the model hatch. A series of spacers

Table 1 Froude scaling factors

Variable	Symbol	Scale factor	Value
Length, in.	L	λ	0.2
Acceleration of gravity, in./s^2	g	1.0	1.0
Mass, slugs	m	λ^3	0.008
Mass moment of inertia, lb/in.^{2}/s^2	J	λ^5	0.00032
Time, s	t	$\lambda^{1/2}$	0.4472
Displacement, in.	x	λ	0.2
Linear velocity, in./s	v	$\lambda^{1/2}$	0.4472
Linear acceleration, in./s	a	1.0	1.0
Angular rotation, rad	θ	1.0	1.0
Angular velocity, rad/s	ω	$\lambda^{-1/2}$	2.236
Angular acceleration, rad/s^2	α	λ^{-1}	5.0

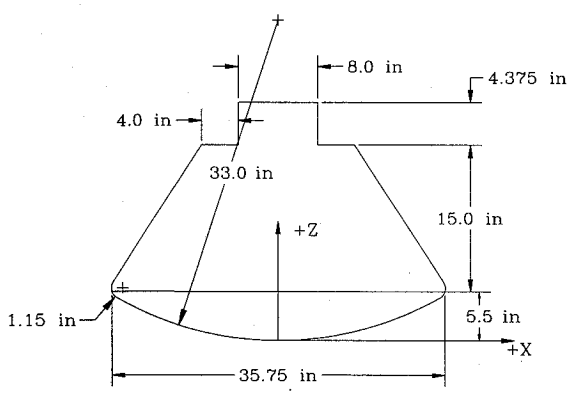

Fig. 1 One-fifth scale WLSM model.

Table 2 Circular plate dimensions for mass moment system

TCH	Inner radius, in.	Outer radius, in.	Thickness, in.
Top plate	0.0	3.0	0.5
Middle plate	4.5	9.0	1.0
Bottom plate	0.0	4.5	1.25

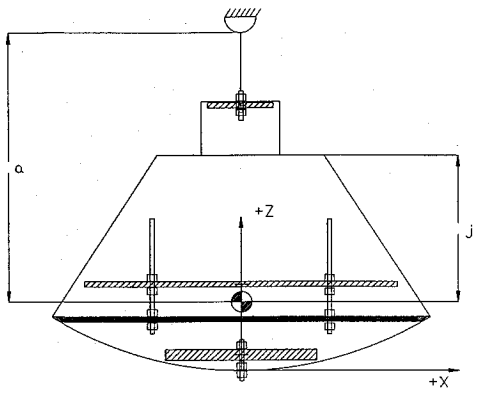

Fig. 2 Mass moment system and pendulum test setup.

on the studs allows vertical variation of the plate. The floor can be rotated 180 deg to permit a total vertical range of approximately 9 in.

Initially the c.g. and moment of inertia of the empty model were determined. Nonhomogeneities of the model shell required empirical determination of the weight, c.g., and mass moment of inertia. The weight was measured by weighing the model on a scale. The total weight of the model with the plate system included was 129 lb. The location of the c.g. and the magnitude of the mass moment of inertia were then measured by suspending the model shell from a 1-ft rod and recording the period of oscillation as it was swung pendulum-like from its top and then from its bottom. The moments in a simple pendulum relationship are summed to determine the equations for the c.g. and mass moment of inertia.[5] Figure 2 shows the pendulum setup with the mass system attached and Eq. (1) describes the pendulum motion:

$$\left(I_G + ma^2\right)\Theta'' + mga\sin\Theta = 0 \tag{1}$$

Assuming small angles, the solution is

$$\Theta = A\sin\left(\sqrt{\frac{mga}{I_G + ma^2}}\,t + \alpha\right) \tag{2}$$

Knowing the natural frequency from Eq. (2), the period was determined:

$$\tau^2 = (k)\left(\frac{I_G + ma^2}{a}\right) \qquad \text{where } k = \frac{4\pi^2}{mg} \tag{3}$$

Swinging the model shell without the mass system from its top and its bottom, the period for each was determined. Equation (3) and the two periods were used to determine the location of the c.g. and the mass moment of inertia about the c.g. of the model shell. This technique generated the following values:

$$Z_{\text{c.g.}} = 8.25 \text{ in. from bottom of model}$$

$$I_G = I_y,\ I_x = 1.701 \text{ lb/in.}^2/\text{s}^2$$

$$X_{\text{c.g.}},\ Y_{\text{c.g.}} = 0.0 \text{ in.}$$

$$I_z = 0.0 \text{ in.}$$

The pendulum test generated the mass moments of inertia about the horizontal axis, I_x and I_y, and the vertical c.g. location. The I_z moment of inertia and horizontal c.g. were not determined. The pitching and rolling motion that the model experiences during the static testing is primarily dependent upon the I_x and I_y moments

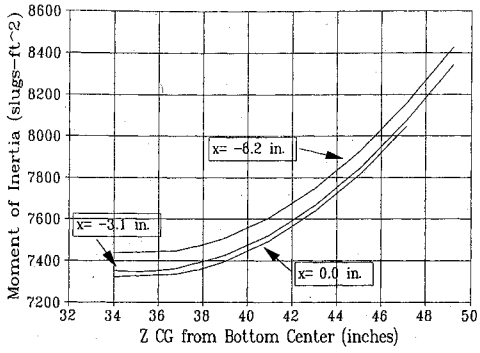

Fig. 3 Mass moment of inertia for varying c.g. location.

of inertia. The pitch and roll motions are about the horizontal axis, so for these tests the I_z moment (the moment about the vertical axis) is not needed. The horizontal c.g. location was assumed to be along the centerline of the model.

Mass Properties

The pendulum test was performed for the model shell only and the other mass properties were determined from an analytical approach. The weight and moment system was added to the model shell to generate the wide range needed for the c.g. Because the weight and location of the centers of mass of all plates are known, the overall c.g., and mass moment of inertia can be determined analytically for any plate position.

The mass center of an object may be obtained from the summation of the mass centers of the system of particles that make up the object.[6] In terms of rectangular coordinates the mass center is

$$Mx = \sum_{i=1}^{n} m_i x_i \qquad My = \sum_{i=1}^{n} m_i y_i \qquad Mz = \sum_{i=1}^{n} m_i z_i \quad (4)$$

Applying the technique in Eq. (4), the x and z mass center locations, or c.g., for the model were obtained for all plate positions.

Knowing the mass and c.g. locations of the model shell and the plate system, the total moment of inertia was obtained through the use of the parallel-axis theorem.[7] The moment of inertia with respect to a given axis of a body made up of several simple shapes may be obtained by computing the moments of inertia of its component parts about the desired axis and then adding them together. Summing the moments of inertia for the plates and the model shell resulted in the moment of inertia of the model. The various c.g. and mass moments of inertia that were generated by the model are scaled up and shown graphically in Fig. 3.

Equations of Dynamic Equilibrium

In water the WLSM can be viewed as a symmetrical, free-floating body, similar to a buoy. Theoretically a craft at sea involves six degrees of freedom, resulting in six equations of motion and six unknowns. The equations of motion for a buoy consist of surge, heave, and pitch. These motions refer to a vehicle traveling in a direction perpendicular to the wave crests. Surge can be assumed to have negligible effects on the motion of a free-floating buoy traveling perpendicular to the wave crest.[8] The equation of dynamic equilibrium was developed in the pitch direction only. Heave motion is not considered in this research and is recommended for future study. The pitch equation of motion was developed for the response of the WLSM in calm seas and several sea states.

Pitch Equation of Motion

The pitch equation of motion was derived from Newton's second law of motion.[6] The moments influencing the model and the equations associated with each of these moments are the following:

$$M_1 = I_w(\theta''), \qquad M_2 = b(\theta'), \qquad M_3 = c\sin(\theta - \phi) \quad (5)$$

The restoring moment M_3 is a product of the restoring force and a moment arm.[9] Referring to Fig. 4, the restoring force can be seen

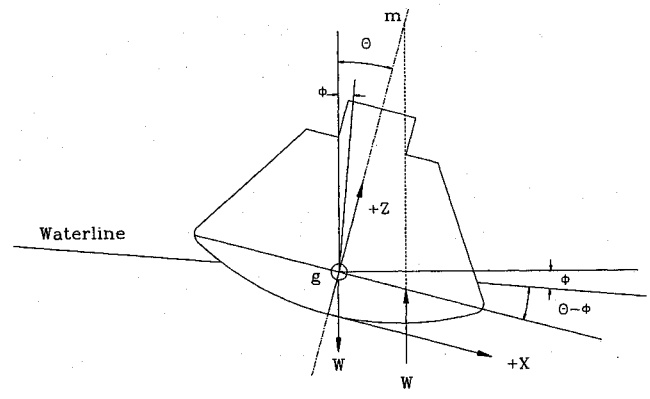

Fig. 4 Pitch or roll oscillations for model.

as the buoyancy force due to an angular deflection. The buoyancy force is the weight W and the moment arm is the distance from the c.g. to the new center of volume of the immersed section. The new center of volume is located at a distance $gm\sin(\theta - \phi)$ from the c.g. The quantity gm can be seen as the distance from the center of gravity to the metacenter m, which is independent of θ for small angles.[10] This distance is referred to as the metacentric height. The relations just described verify that the restoring moment coefficient c equals Wgm and that c is constant for small angles.

The added inertia term I is the moment of inertia of the water entrained by the model.[11] The moments on the model can be summed to generate the following equation:

$$\sum M = I_w(\theta'') + b(\theta') + c\sin(\theta - \phi) = 0 \quad (6)$$

Assuming small angle approximation for $c\sin(\theta - \phi) = c(\theta - \phi)$ and expressing the wave slope as

$$\phi = \alpha_m \sin(\omega t) \quad (7)$$

where, $\alpha_m = \pi(h/L)$.[12] Equation (6) may be rearranged by placing the model terms on the left and the wave term on the right:

$$I_w(\theta'') + b(\theta') + c\theta = c\alpha_m \sin(\omega t) \quad (8)$$

The right-hand side of Eq. (8) represents the exciting force caused by the wave. To solve for the unknown quantities the homogeneous equation for the model can be written as

$$\theta'' + (b/I_w)\theta' + (c/I_w)\theta = 0 \quad (9)$$

Equation (9) is analogous to the general harmonic equation of a mass spring damper system[13]:

$$\theta'' + 2\zeta\omega_n\theta' + \omega_n^2\theta = 0 \quad (10)$$

Equating Eqs. (9) and (10) provides a relationship for b and c:

$$b = 2\zeta\omega_n(I_w) \quad (11)$$

$$c = w_n^2(I_w) \quad (12)$$

In naturally occurring systems there is some damping present. With the presence of damping in the system, $0 < \zeta < 1$, the solution to Eq. (10) is

$$\theta_h = e^{-\zeta\omega_n t}\left[A\cos\left(\omega_n\sqrt{1-\zeta^2}t\right) + B\sin\left(\omega_n\sqrt{1-\zeta^2}t\right)\right] \quad (13)$$

The unknown constants A and B are determined from initial conditions: the initial angle and angular velocity at time zero. The variables ω_n and ζ are developed from static pool tests.

The exciting force for the steady-state pitch motion is due to the moment exerted by the wave on the model, represented by the sinusoidal motion of Eq. (8). From Eq. (8), the forced motion with the model terms and wave terms incorporated becomes

$$\theta'' + (b/I_w)\theta' + (W\overline{gm}/I_w)\theta = (W\overline{gm}/I_w)\alpha_m \sin(\omega t) \quad (14)$$

Equation (14) can be solved in terms of the damping factor and the undamped natural frequency with the left side the same as Eq. (10), and the right side unchanged. Equation (14) has a general solution of the following form[13]:

$$\theta = \theta_h + \theta_a \sin(\omega t - \epsilon) \tag{15}$$

where

$$\theta_a = \frac{\alpha_m \omega_n^2}{\sqrt{\left(\omega_n^2 - \omega^2\right)^2 + 4\zeta^2\omega_n^2\omega^2}} \tag{16}$$

$$\epsilon = \tan^{-1}\left(\frac{2\zeta\omega_n\omega}{\omega_n^2 - \omega^2}\right) \tag{17}$$

The pitching motion consists of the natural and forced oscillations. The natural oscillations contain the frequency of the model in still water and an exponential decaying term, Eq. (13). The exponential term causes the natural response to die out with time. The forced oscillations have amplitude θ_a and a phase shift ϵ that do not change with time and do not depend upon the initial conditions of the model. The steady-state condition results in

$$\theta = \theta_a \sin(\omega t - \epsilon) \tag{18}$$

Comparing the steady state with the exciting moment for pitch, there is a phase difference between the model motion and the exciting moment. In Eq. (18) if there is no damping, and thus no phase shift; the model motion occurs simultaneously with the exciting moment.

Static Pool Tests

The static pool tests were conducted on the clean model with a variety of c.g. locations. The attitude spheres were then added to the model, and the same c.g. locations were tested with the attitude spheres. The results of the tests were used to determine the coefficients in the pitch equation of motion.

Clean Model

Static pool tests determined the damping factor and the natural frequency of the clean model in pitch. For each model c.g. location tested, the model was displaced approximately 20 deg in a static pool. The model was then released and allowed to oscillate until it came to rest. Three tests were performed for each model configuration to determine an average response.

The oscillations were recorded on video tape in real time. The VHS tape was then time coded. The time-coding process displays the real time on the screen in hours, minutes, seconds, and frame number. The tape speed is 30 frames per s. The number of frames between oscillations was counted to determine the damped natural period. This process provided an accuracy of $\pm 1/30$th of a second in calculating the period. The small time-step helps eliminate the human error associated with reaction times.

The angular displacement for several successive pitch peaks was measured from the monitor screen. The values of ζ and ω_n were evaluated by applying the formula for the logarithmic decrement that is the natural logarithm of the ratio of two successive amplitudes of oscillation.[14] The value of the logarithmic decrement is the same for any two successive peaks in a system with viscous damping. The assumption of viscous damping allows the application of the logarithmic decrement to the experimental values.[8] The equations used in determining the coefficients from the static testing are listed below:

$$\delta = \ell n(\theta_1/\theta_2) = \ell n(e^{\zeta\omega_n T_d}) = \zeta\omega_n T_d \tag{19}$$

where θ_1 and θ_2 are pitch peaks,

$$\omega_n = \frac{2\pi}{T_d\sqrt{1-\zeta^2}} \tag{20}$$

$$\zeta = \sqrt{\frac{\delta^2}{4\pi^2 + \delta^2}} \tag{21}$$

Table 3 Experimental data calculated from static pool tests

$Z_{c.g.}$	$X_{c.g.}$	Period, s (T_d)	Natural freq., rad/s (ω_n)	Damping factor (ζ)
9.84	1.24	1.137	5.544	0.0823
8.19	1.24	0.912	6.917	0.0904
7.78	1.24	0.889	7.129	0.1308
7.36	1.24	0.9268	6.829	0.1197
6.79	1.24	0.911	6.943	0.1149
9.84	0.62	1.067	5.912	0.090
9.01	0.62	1.020	6.201	0.114
8.19	0.62	0.9165	6.899	0.1118
7.78	0.62	0.885	7.142	0.1067
7.36	0.62	0.8657	7.326	0.1364
6.79	0.62	0.8492	7.424	0.0810
9.84	0.0	1.030	6.147	0.123
9.01	0.0	0.983	6.424	0.0971
8.60	0.0	0.927	6.824	0.1163
7.78	0.0	0.928	6.796	0.0869
7.36	0.0	0.9092	6.962	0.1214
6.79	0.0	0.8633	7.327	0.1153

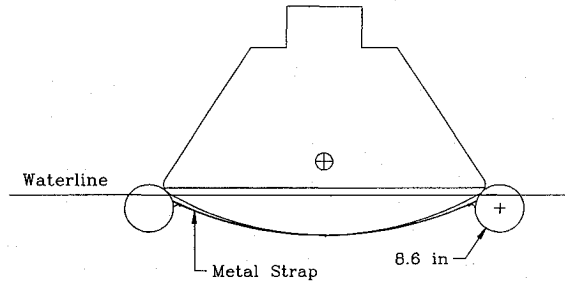

Fig. 5 Attitude sphere attachment.

The resulting coefficients determined from the static testing are listed in Table 3. The coefficients enable prediction of pitch response of the model in a given sea state condition without determining the added inertia of the model. The added inertia term is difficult to calculate and can be avoided using model testing and the assumption of viscous damping.

Model with Stabilization Aids

The model with stabilization aids is the clean model with attitude spheres attached just below the waterline. Figure 5 illustrates how the attitude spheres were attached to the model with metal straps. The straps were affixed to the model to provide a rigid attachment point for the spheres.

The test model was subjected to three different attitude sphere configurations, ranging from a nominal case of six spheres to an off-nominal case of three. The first configuration was symmetrical and consisted of six spheres located every 60 deg. The second consisted of four spheres in a symmetrical configuration with the spheres located at 30, 150, 210, and 330 deg, with the center of the hatch being the 0-deg mark. The third testing configuration consisted of three spheres in an unsymmetrical configuration about the x–z plane located at 30, 210, and 270 deg. The sphere volume for a prototype WLSM was assumed to be 24 ft^3. The 24 ft^3 volume scales down to a sphere diameter of 8.6 in. for the model's attitude spheres.

The equations developed for the clean model were applied to the model with attitude spheres. The model was evaluated with the same assumptions that damping was viscous and that the restoring moment coefficient remained constant, $c = Wgm$. Therefore, the evaluation of the model with attitude spheres attached consisted of static pool experiments under different c.g. locations and different sphere locations.

The pitch experiments were carried out in the same manner as those for the clean model. Static pool tests were used to determine T_d and the pitch peaks for the model. For each experiment, the model was placed in the static pool and displaced approximately 20 deg. The model was then released and allowed to oscillate until it came to rest. The model was tested at each c.g. location three times. For each c.g. location the number of attitude spheres was varied from 6 to 4, and then to 3. The oscillations were recorded on video tape

Table 4 Coefficients for model with spheres at $X_{c.g.}$ = 1.24 in.

$Z_{c.g.}$	$X_{c.g.}$	Spheres	Period, s (T_d)	Natural freq., rad/s (ω_n)	Damping factor (ζ)
9.84	1.24	0	1.137	5.544	0.0823
9.84	1.24	4	0.9185	6.802	0.1656
9.84	1.24	6	0.9722	6.524	0.1356
8.60	1.24	3	0.9208	6.883	0.1252
8.60	1.24	4	0.933	6.756	0.0956
8.19	1.24	0	1.044	6.115	0.1691
8.19	1.24	3	0.871	7.257	0.1092
8.19	1.24	4	0.924	6.835	0.1036
8.19	1.24	6	0.950	6.659	0.1098
7.78	1.24	0	1.007	6.298	0.1356
7.78	1.24	3	0.907	6.963	0.0950
7.78	1.24	4	0.956	6.687	0.1806
7.78	1.24	6	0.919	6.903	0.1376
7.36	1.24	0	1.047	6.044	0.1103
7.36	1.24	3	0.933	6.852	0.1686
7.36	1.24	4	0.898	7.045	0.1315
7.36	1.24	6	0.90	7.054	0.124
6.79	1.24	0	0.967	6.578	0.152
6.79	1.24	3	0.960	6.610	0.133
6.79	1.24	4	0.938	6.750	0.123
6.79	1.24	6	0.967	6.589	0.1632

Table 5 Coefficients for model with spheres at X_{cg} = 0.62 in.

$Z_{c.g.}$	$X_{c.g.}$	Spheres	Period, s (T_d)	Natural freq., rad/s (ω_n)	Damping factor (ζ)
9.84	0.62	0	1.067	5.912	0.0896
9.84	0.62	3	0.967	6.435	0.1464
9.84	0.62	4	0.933	6.850	0.1816
9.84	0.62	6	0.933	6.794	0.1306
9.01	0.62	0	1.02	6.201	0.1136
9.01	0.62	3	0.947	6.679	0.1136
9.01	0.62	4	0.927	6.878	0.1619
9.01	0.62	6	0.907	6.627	0.1743
8.19	0.62	3	0.920	6.930	0.1664
8.19	0.62	4	0.952	6.720	0.1882
8.19	0.62	6	0.905	6.999	0.1250
7.78	0.62	3	0.940	6.855	0.2080
7.78	0.62	4	0.900	7.094	0.167
7.78	0.62	6	0.933	6.853	0.1820
6.79	0.62	3	0.927	6.856	0.1358
6.79	0.62	4	0.933	6.852	0.1840
6.79	0.62	6	0.933	6.887	0.2074

Table 6 Coefficients for model with spheres at $X_{c.g.}$ = 0.0 in.

Z_{cg}	X_{cg}	Spheres	Period, s (T_d)	Natural freq., rad/s (ω_n)	Damping factor (ζ)
9.84	0.0	0	1.03	6.147	0.1235
9.84	0.0	3	0.951	6.669	0.1359
9.84	0.0	4	0.956	6.652	0.1540
9.84	0.0	6	0.921	6.899	0.1478
9.01	0.0	0	0.983	6.424	0.0971
9.01	0.0	3	0.933	6.793	0.1244
9.01	0.0	4	0.942	6.722	0.1054
9.01	0.0	6	0.933	6.819	0.1567
8.19	0.0	0	0.960	6.575	0.0946
8.19	0.0	3	0.933	6.770	0.0953
8.19	0.0	4	0.914	6.928	0.1245
8.19	0.0	6	0.911	7.014	0.1817
7.78	0.0	3	0.927	6.809	0.0931
7.78	0.0	4	0.946	6.732	0.1565
7.78	0.0	6	0.922	6.919	0.1690
6.79	0.0	3	0.927	6.860	0.1451
6.79	0.0	4	0.942	6.766	0.1641
6.79	0.0	6	0.922	6.874	0.1251

in real time. The period and pitch peaks, θ_1, θ_2, etc., were measured from the video tape in the same manner as the clean model tests. The coefficients were then determined using Eqs. (19–21). The results for the sphere model are listed in Table 4 for the maximum offset horizontal c.g. ($X_{c.g.}$ = 1.24 in.), Table 5 for the middle offset ($X_{c.g.}$ = 0.62 in.), and in Table 6 for the zero offset ($X_{c.g.}$ = 0.0 in.).

Results and Calculations

The magnification factor μ, a measure of dynamic response, is the ratio of the amplitude in the dynamic case to that in the static case.[12] The tuning factor Λ is the ratio of the wave frequency to the model's natural frequency, $\Lambda = \omega/\omega_n$. Plotting the magnification factor vs the tuning factor indicates how much the amplitude of the model is increased by the dynamic effects of the wave motion. The magnification factor is evaluated from Eq. (16). The coefficient θ_a is the dynamic variable and α_m is the static variable. The magnification factor equation is nondimensional and, represented in terms of Λ and ζ, is

$$\mu = \frac{\theta_a}{\alpha_m} = \frac{1}{\sqrt{(1-\Lambda^2)^2 + (2\zeta\Lambda)^2}} \tag{22}$$

The wave series values used in the forcing function, Eq. (8), are listed in Table 7. Wave series 1–4 represent the scaled down values of sea states 2–4, with wave series 1 and 2 representing high and low frequencies of sea state 2.

Clean Model

The free pitch response of the model is generated by substituting in the corresponding ζ and ω_n terms into the free response pitch solution, Eq. (13). Varying the $Z_{c.g.}$ while holding the $X_{c.g.}$ at zero had little effect on the free pitch response. The free response of the model does not change significantly with a varying $Z_{c.g.}$.

Figure 6 is a plot of the model in free oscillation with the $Z_{c.g.}$ fixed at 7.78 in. and the $X_{c.g.}$ varied from 0.0 to 1.24 in. The greatest pitch motion is experienced at $X_{c.g.}$ location of 0.0 in. The pitch motion is reduced as the $X_{c.g.}$ is offset from zero. This result can be expressed physically in the sense that the displaced model will want to stay to the offset c.g. side and not pitch back. The model has increasing inertia as the $X_{c.g.}$ offset increases. This increase in inertia and different c.g. position changes the natural frequency of the model.

The pitch response for Eq. (18) is shown in Fig. 7. The figure shows the results of varying the $Z_{c.g.}$, while the $X_{c.g.}$ is held constant. The forcing function is wave series 4 from Table 7. The response shows that the pitching motion is reduced and that there is a small amount of phase shift for the c.g. positions displayed. The response does not change significantly with varying $Z_{c.g.}$.

Figure 8 is a plot of the forced pitch response of the model under wave series 4 with a maximum $Z_{c.g.}$ of 9.84 in. and a varying $X_{c.g.}$. Wave series 4 has a height of 1.2 ft and frequency of 2.83 rad/s. The pitch amplitude of the model is increasing with the $X_{c.g.}$ offset. This is opposite of the observation for Fig. 6. The wave action induces a continuous motion, and the inertia keeps the model pitching, causing the pitch motion under a sea state to increase as the $X_{c.g.}$ is offset.

Table 7 Wave series values

Wave series	Wave height, ft	Wave frequency, rad/s	Wave length, ft
1	0.4	6.91	4.23
2	0.4	4.71	6.42
3	0.8	3.52	16.4
4	1.2	2.83	25.0

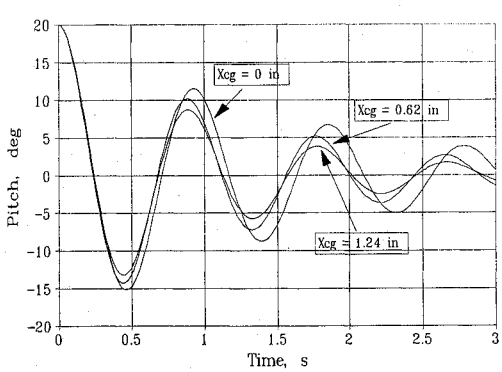

Fig. 6 Free pitch response with variable $X_{c.g.}$ and fixed $Z_{c.g.}$ at 7.78 in.

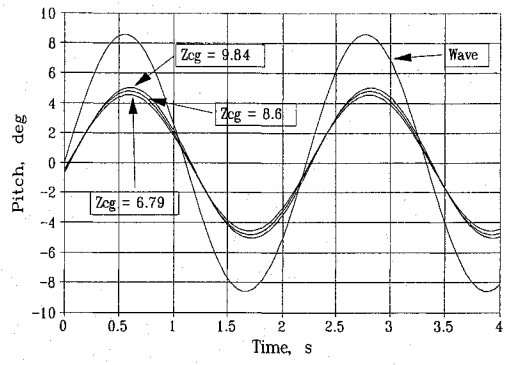

Fig. 7 Forced pitch response in wave series 4 with $X_{c.g.}$ = 0.0 in. and $Z_{c.g.}$ from 6.79 to 9.84 in.

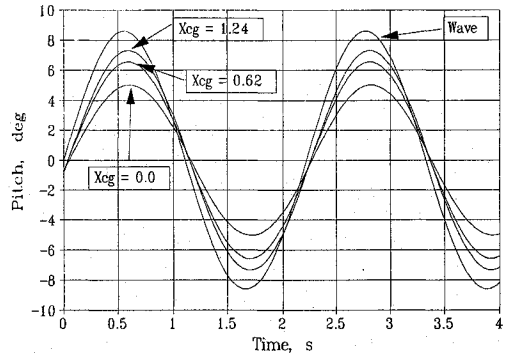

Fig. 8 Forced pitch response in wave series 4 with $X_{c.g.}$ from 0.0 to 1.24 in. and $Z_{c.g.}$ = 9.84 in.

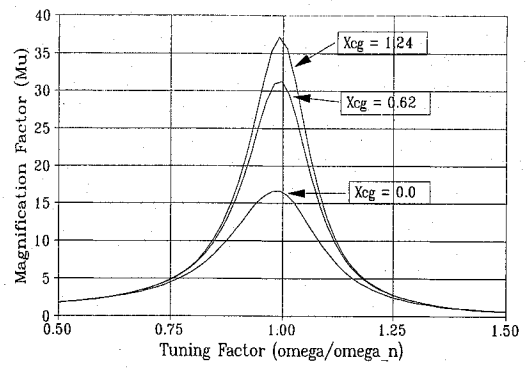

Fig. 9 Magnification factor vs tuning factor with $X_{c.g.}$ from 0.0 to 1.24 in. and $Z_{c.g.}$ = 9.84 in.

Figure 9 is a plot of the magnification factor vs tuning factor for a $Z_{c.g.}$ of 9.84 in. held constant and varying the $X_{c.g.}$. The plot shows that when the frequency of the wave approaches that of the model, the value of the magnification factor reaches a maximum. The derivative with respect to Λ is taken, and set equal to zero to obtain the true maximum of Eq. (22). This yields the relationship for the maximum, $\Lambda = (1-\zeta^2)^{1/2}$. This relationship shows that the magnification factor is a maximum at a value of Λ slightly less than 1, depending upon the magnitude of ζ. This condition is noticeable in Fig. 9. As damping increases, moving from the maximum to the minimum $Z_{c.g.}$, the peak is reduced and shifted to the left. The effect of the damping factor is more pronounced near resonance. The damping factor reduces the peaks at resonance.

Figure 10 is a plot of the magnification factor vs the tuning factor for an $X_{c.g.}$ of 0.0 in., and the $Z_{c.g.}$ varied from its minimum to maximum position. There was no trend noticed in the magnitude of the peaks, and they appear random. The peaks are directly related to the damping factor and for these c.g. locations there was no consistency in the damping characteristics. The only trend noticed is the location of the peaks, which occur near resonance.

The model's natural frequency increases as the $Z_{c.g.}$ is lowered, resulting in resonance occurring at higher frequencies. This condition means the model can float in a larger range of sea states and not encounter resonance. The high-frequency wave (wave series 1 from Table 7) is the only wave series that has a frequency in the range of the clean model's natural frequencies, listed in Table 3.

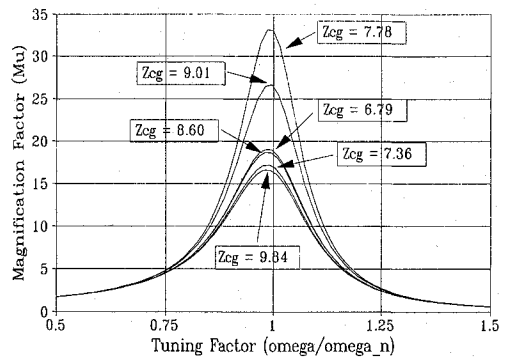

Fig. 10 Magnification factor vs tuning factor with $X_{c.g.}$ = 0.0 in. and $Z_{c.g.}$ from 6.79 to 9.84 in.

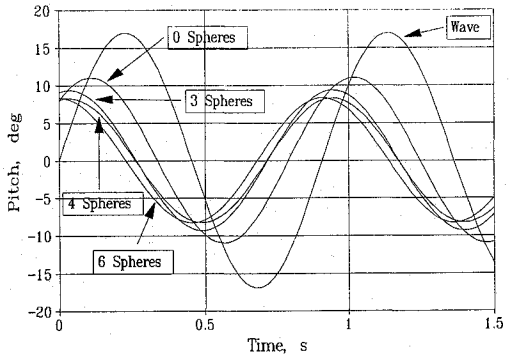

Fig. 11 Forced pitch response with attitude spheres in wave series 1 with $X_{c.g.}$ = 0.0 in. and $Z_{c.g.}$ = 9.84 in.

Model with Stabilization Aids

The equations of motion developed were applied to the modified model. The additional mass the spheres add to the model was assumed negligible. Trends for the model with attitude spheres were more recognizable in the static test results than when the coefficients are averaged and applied to the free response equation. To obtain results for the forced equation, the coefficients were averaged and subjected to the different wave series listed in Table 7.

The static test results verified that the attitude spheres offered increased pitch damping for all three sphere configurations. The only additional effect the three sphere arrangement had on the free response was to reduce the static draft angle. This reduction in the static draft caused the model to oscillate about a new, smaller, static draft angle.

The averaged coefficients evaluated from the static pool tests were applied to the forced pitch equation to produce the forced pitch response shown in Fig. 11. The varied response of the model is a result of the addition of the attitude spheres attached to the model. The spheres decrease the forced pitching motion of the model. As the number of spheres increased, the pitch amplitude decreased. The increasing number of spheres also has an effect on the phase shift. As the number of spheres increased, the phase lag between the wave motion and the model motion was increased. Wave series 1 from Table 7 is the wave forcing function in Fig. 11.

In Fig. 12, the magnification factor vs the tuning factor is plotted at a c.g. position of 0.0 in., 9.84 in., with the number of attitude spheres being varied from zero to six. The attitude spheres reduced the amplitude of the magnification factor. The lower the peak, the lower the pitch amplitude in the wave series.

The attitude spheres increased the damping factor for the model. Figure 12 shows there was no significant difference between the four- and six-sphere configurations. This result suggests that increasing the number of spheres beyond four is not effective.

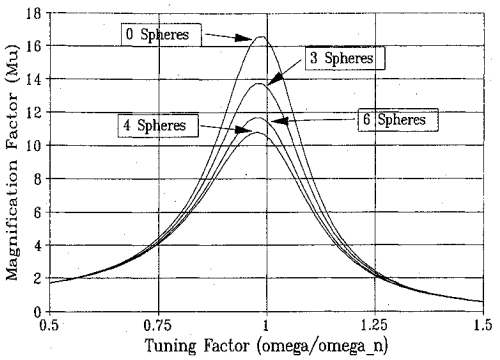

Fig. 12 Magnification factor vs tuning factor with attitude spheres with $X_{c.g.}$ = 0.0 in. and $Z_{c.g.}$ = 9.84 in.

The addition of the attitude spheres also increased the natural frequency of the model. These values are available in Tables 4–6. The ability to change the natural frequency allows some control over the occurrence of resonance. Landing in a sea state with a frequency equal to the clean model's frequency can generate resonance. Through the addition of attitude spheres, the resonance condition could be avoided by changing the natural frequency of the model. This ability allows a WLSM to increase its possible landing sites, by increasing the sea states in which it can land without resonance occurring.

Observations and Recommendations

In this research, the stability of a WLSM model in pitch motion was investigated. Using the equations of motion for buoys, the natural pitch characteristics of the WLSM model were determined through static pool testing. Resulting characteristics were then used in the pitch equations to identify the motion of the model. Free response pitch motion of the model damped out quickly, and the magnitude of free pitch motion decreased with an increasing offset of the model's c.g. Forced pitch amplitude increased with the increasing $X_{c.g.}$ offset, moving closer to the wave amplitude. The forced pitch response did not change significantly with varying $Z_{c.g.}$ with the pitch motion remaining less than the forcing wave's motion.

The same test process used for the clean model was applied to the model with attitude spheres attached. The model was tested experimentally with the spheres in a symmetrical arrangement of six and four, and in an unsymmetrical arrangement of three. The free response pitch motion of the model damped out sooner with the attitude spheres. The unsymmetrical arrangement of three spheres reduced the static draft angle, resulting in a shift of the free response to oscillate about the new static draft angle.

The addition of spheres reduced the amplitude of the forced response pitching motion. The natural frequency of the model increased with the increasing number of attitude spheres. The phase shift was increased with the addition of the attitude spheres, as shown in the forced response plots. The damping coefficient of the model without attitude spheres ranged from 0.08 to 0.13, and for the model with attitude spheres from 0.09 to 0.20. The attitude spheres did not provide a significant increase in damping. If the WLSM is to incorporate a flotation system, such as the attitude spheres, storage and deployment techniques need to be developed in future research.

The model is in a resonant wave state when the model's natural frequency is the frequency of the wave. The resonant condition induces an increase in pitch oscillation amplitude. Because the WLSM is essentially an unpowered free-floating buoy, it cannot control its speed or direction to change the frequency of the oncoming waves. A solution to avoiding resonance is to alter the craft's natural frequency away from the frequency of the oncoming waves. Two ways of altering the natural frequency were revealed in the research: 1) change the craft's c.g. position or 2) add attitude spheres. Human tolerance levels, human effectiveness levels, and rescue procedures become increased considerations if the craft's natural frequency cannot be altered enough to avoid resonance. Rigidly attached attitude spheres increase damping and change the natural frequency in pitch.

Acknowledgments

A portion of this work was supported by NASA and the University Space Research Association, to whom appreciation is expressed. Appreciation is expressed to Rockwell Space Systems Division for supporting the Rockwell Graduate Fellowships that made this work possible. The authors gratefully acknowledge the assistance of Raymond C. Manion, W. Robert Mason, Peter Kondis, Don Morris, and John McKinney of Rockwell International's Space Systems Division in preparing this document and discussing many of the testing ideas contained herein.

References

[1]Albano, E., and Pohlen, M. J., "A Method for Determining the Dynamics of the Apollo Command Module at Sea," North American Aviation, SID 63-466, Downey, CA, May 1963.

[2]Theurich, A., "Apollo Postlanding Crew Survival: Land or Water Impact," North American Aviation, SID 64-778, Downey, CA, May 1964.

[3]White, R. D., "Apollo Experience Report Command Module Uprighting System," NASA TN D-7081, March 1973.

[4]Baker, W. I., Westine, P. S., and Dodge, F., *Similarity Methods in Engineering Dynamics*, Hayden, Rochelle Park, NY, 1973, pp. 92, 93.

[5]Greenwood, D. T., *Principles of Dynamics*, 2nd. ed., Prentice–Hall, Englewood Cliffs, NJ, 1988, pp. 362, 363.

[6]Beer, F. P., and Johnston, E. R., Jr., *Vector Mechanics for Engineers: Dynamics*, 5th ed., McGraw–Hill, New York, 1988, pp. 657–661.

[7]Beer, F. P., and Johnston, E. R., Jr., *Vector Mechanics for Engineers: Statics*, 4th ed., McGraw–Hill, New York, 1984, pp. 368–370.

[8]Comstock, J. P. (ed.), *Principles of Naval Architecture*, Society of Naval Architects and Marine Engineers, New York, 1967, pp. 628, 633.

[9]Gillmer, T. C., *Modern Ship Design*, United States Naval Inst., Annapolis, MD, 1970, p. 92.

[10]White, R. D., *Fluid Mechanics*, 2nd ed., McGraw–Hill, New York, 1986, pp. 78, 79.

[11]Berteaux, H. O., *Buoy Engineering*, Wiley, New York, 1976, pp. 59–61.

[12]Bhattacharyya, R., *Dynamics of Marine Vehicles*, Wiley, New York, 1978, pp. 33, 38.

[13]James, M. L., Smith, G. M., Wolford, J. C., and Whaley, O. W., *Vibration of Mechanical and Structural Systems: With Microcomputer Applications*, Harper & Row, New York, 1989, pp. 55–58, 137–140.

[14]Thomson, W. T., *Theory of Vibrations with Applications*, Prentice–Hall, Englewood Cliffs, NJ, 1988, p. 33.

T. C. Lin
Associate Editor